

A Bayesian method for estimating gene-level polygenicity under the framework of transcriptome-wide association study

Arunabha Majumdar^{1*} and Bogdan Pasaniuc^{2*}

¹Department of Mathematics, Indian Institute of Technology Hyderabad, Kandi, Telangana, India

²Department of Pathology and Laboratory Medicine, University of California Los Angeles, California, USA

*Correspondence: arun.majum@math.iith.ac.in (AM), pasaniuc@ucla.edu (BP)

arXiv:2207.12173v1 [q-bio.GN] 25 Jul 2022

Abstract

Polygenicity refers to the phenomenon that multiple genetic variants have a non-zero effect on a complex trait. It is defined as the proportion of genetic variants that have a nonzero effect on the trait. Evaluation of polygenicity can provide valuable insights into the genetic architecture of the trait. Several recent works have attempted to estimate polygenicity at the SNP level. However, evaluating polygenicity at the gene level can be biologically more meaningful. We propose the notion of gene-level polygenicity, defined as the proportion of genes having a non-zero effect on the trait under the framework of transcriptome-wide association study. We introduce a Bayesian approach *polygene* to estimate this quantity for a trait. The method is based on spike and slab prior and simultaneously provides an optimal subset of non-null genes. Our simulation study shows that *polygene* efficiently estimates gene-level polygenicity. The method produces downward bias for small choices of trait heritability due to a non-null gene, which diminishes rapidly with an increase in the GWAS sample size. While identifying the optimal subset of non-null genes, *polygene* offers a high level of specificity and an overall good level of sensitivity – the sensitivity increases as the sample size of the reference panel expression and GWAS data increase. We applied the method to seven phenotypes in the UK Biobank, integrating expression data. We find height to be most polygenic and asthma to be the least polygenic. Our analysis suggests that both HDL and triglycerides are more polygenic than LDL.

Introduction

Beyond the discovery of genetic loci associated with a complex trait, it is crucial to estimate the overall distribution of the effect size of genome-wide genetic variants to understand the genetic architecture of the trait better [1]. Polygenicity is the proportion of genetic variants that have a nonzero effect on the trait. It is an essential characteristic of the effect size distribution and provides valuable insights into the genetic architecture of the trait. Efficient estimation of this quantity can help to improve the design of risk prediction models [2] or reveal the biological complexity of a trait [3]. Several approaches have attempted to estimate the polygenicity using its definition as the proportion of single nucleotide polymorphisms (SNPs), which have a nonzero effect on the trait under the framework of genome-wide association study (GWAS) [1,4]. We refer to it as the SNP-level polygenicity. However, defining polygenicity at a gene level can be biologically more meaningful. In this paper, we propose the notion of gene-level polygenicity, which we define as the proportion of genes that have a nonzero effect on the trait. An expression data set containing data on the trait of interest would be ideal for estimating the gene-level polygenicity. However, most expression data sets have a limited sample size, and the data on various quantitative or disease traits may not be available.

Even though GWASs have discovered many common genetic variants associated with the risk of complex traits, most of these variants reside in non-coding genomic regions, making the functional interpretation of the GWAS signals challenging. Since the common variants associated with a complex trait tend to co-localize with expression quantitative trait loci (eQTLs) of the causal genes for the trait, a promising alternative approach is the transcriptome-wide association studies (TWAS) [5,6]. TWAS integrates reference panel expression (and genotype) data with GWAS data to test for an association between the predicted genetic component of expression and a trait. Such studies combine eQTL effects estimated from the reference panel expression data and summary statistics from a GWAS. TWAS has identified numerous novel gene-trait associations and offers better biological interpretation than GWAS [7]. Furthermore, it can be implemented efficiently using summary-level association data only [6].

Considering the above deliberations, we develop a statistical approach to estimate the gene-level polygenicity under the framework of TWAS using summary-level association data. While evaluating SNP-level polygenicity, a crucial step is to account for the linkage disequilibrium (LD) among SNPs and identify the SNPs which originally have a nonzero effect [1,4]. Two current methods, Genesis [1] and BEAVR [4], estimate the number/proportion of susceptibility SNPs for a trait while taking into account LD structure. Genesis forecast the number of non-zero effect SNPs at a genome-wide level [1] which can be converted into a proportion of non-null SNPs. BEAVR partitions the genome into regions and estimates regional polygenicity [4]. A marginally associated SNP may not always have a nonzero effect. Instead, it may be in LD with an SNP, which has a nonzero effect. Similarly, a marginally associated gene in TWAS may not originally have a nonzero effect.

Instead, the marginal association may be due to a correlation between the predicted expression of the gene and another gene (gene co-regulation) where the latter truly has a nonzero effect. Such correlation between two genes' predicted expression can arise due to shared eQTLs or LD between eQTLs of the genes [8]. We develop a Bayesian approach to estimate the proportion of genome-wide genes, the genetic component of expressions of which have a nonzero effect on the trait (non-null genes). We consider this proportion of non-null genes as a measure of gene-level polygenicity. We estimate the proportion of non-null genes explicitly accounting for correlation between the predicted genetic components of expressions. Our unified Bayesian framework also simultaneously provides an optimal subset of non-null genes. We refer to the method as *polygene* (*polygenicity at gene level*). We consider a continuous spike and slab prior to develop *polygene* [9–12]. The spike component represents the null effect, and the slab component represents the non-null effect. We perform a fully Bayesian inference based on MCMC while explicitly accounting for the covariance structure among the genes. Furthermore, the method uses marginal TWAS summary statistics, which are often publicly available.

We perform extensive simulations to evaluate the performance of the approach. *polygene* efficiently estimates the gene-level polygenicity under various simulation scenarios. It produces a downward bias in the estimation when the heritability per non-null gene is small. The downward bias decreases rapidly as the GWAS sample size increases. Simulations also show that the q-value approach implemented in this context consistently produces a sizeable upward bias in all simulation scenarios. While identifying the optimal subset of non-null genes, *polygene* offers high specificity and good sensitivity across the simulation scenarios. The sensitivity improves with an increase in the sample size of the reference panel expression and GWAS data. We applied *polygene* to seven traits in the UK Biobank integrating expression data. Our analysis shows that height is the most polygenic, and asthma is the least polygenic. We also observe that both HDL and triglycerides are more polygenic than LDL.

Material and methods

Overview of methods

The standard TWAS consists of two-stage regressions. In the first stage, we consider a tissue of interest in the reference panel of expression (and genotype) data. We fit a penalized regression [13, 14] to evaluate the effect of genotypes of SNPs surrounding the gene (local SNPs) on the expression. From the regression for each gene, we obtain a prediction model to estimate the genetic component of the gene's expression based on its local SNPs. In the second stage, we use the prediction model to predict the genetic component of expression in the GWAS data based on the same set of local SNPs. We then regress a GWAS trait on the predicted expression to assess an association between the gene and the trait. We repeat this pipeline to obtain the marginal

TWAS statistics for all the genes. Next, we derive the analytic formulas of the expectation vector and covariance matrix for the TWAS statistics of all genes. We assume a multivariate normal distribution of the TWAS statistics for the genes on each chromosome. Our main goal is to estimate the proportion of all such genome-wide genes which have a non-zero effect on the trait (gene-level polygenicity). We also aim to identify the optimal subset of non-null genes. To model sparsity, we consider a continuous spike and slab prior distribution [9,12] for the TWAS effect sizes and develop a unified Bayesian approach to perform both the estimation of gene-level polygenicity and selection of non-null genes. With prior probability p , the TWAS effect size follows the slab distribution representing a non-null effect. In the data likelihood, we explicitly account for the covariance structure of genes. We derive the full-conditional posterior distributions of the model parameters to implement MCMC using the Gibbs sampling. Finally, we perform Bayesian inference based on the posterior sample of the model parameters obtained by the MCMC.

Regression of gene expression on local SNPs in reference panel

We describe the main steps of *polygene* for m genes on a single chromosome, the extension of which for all chromosomes is straightforward. In the reference panel data, we regress the expression of j^{th} gene on the genotypes of its local SNPs (e.g., SNPs within 0.5 MB window of the gene boundary), $j = 1, \dots, m$. We consider the following linear model:

$$E_j = \mathbf{x}'_j \mathbf{w}_j + \epsilon_j \tag{1}$$

E_j denotes the mean-centered expression of j^{th} gene in the specific tissue of interest. For the local SNPs, \mathbf{x}_j denotes the normalized genotype vector (centered for mean and then scaled by standard deviation) and \mathbf{w}_j denotes the effect size vector, ϵ_j denotes the random error. Since the number of local SNPs can be close to or larger than the sample size of the reference panel (e.g., GTEx data [15,16]), we implement a penalized regression (e.g., Lasso [13], Elastic Net [14]) to estimate \mathbf{w}_j individually for each $j = 1, \dots, m$. Suppose, we have r_j local SNPs for j^{th} gene. Let r denote the total number of unique SNPs considered for the m genes, and the SNPs are arranged in increasing order of base pair positions. Consider $r \times m$ matrix: $\hat{W} = [\hat{\mathbf{w}}_1, \dots, \hat{\mathbf{w}}_m]$. For j^{th} gene, all entries of $\hat{\mathbf{w}}_j$ are zero except for the r_j local SNPs. Note that some of the r_j entries can be zero due to fitting a penalized regression (e.g., Lasso). For each of these m genes, we also assume that the local SNPs produced a significantly positive heritability of expression. We term such a gene as a locally heritable gene. We drop a gene from the downstream analysis if it is not locally heritable.

Regression of trait on predicted expression in GWAS data

In general, expression measurements are not available in GWAS data. Suppose the genotype data for the set of local SNPs considered for a gene in the reference panel is also available in GWAS data.

In that case, we can predict the genetic component of the gene's expression using \hat{W} (obtained in the first stage regression). We estimate the genetic component of expression for m genes as: $\hat{\mathbf{G}} = X\hat{W}$. $X_{n \times r}$ is the genotype matrix for n individuals and r local SNPs in the GWAS data. The genotype data of each SNP is normalized to have zero mean and unity variance. Subsequently, we can perform a multiple linear regression of a continuous GWAS trait Y on $\hat{\mathbf{G}}$ to evaluate the joint effect of the m genes on Y as:

$$Y = \hat{\mathbf{G}}\boldsymbol{\alpha} + \mathbf{e} \quad (2)$$

Y denotes the trait vector for n individuals. $\boldsymbol{\alpha} = (\alpha_1, \dots, \alpha_m)'$ denotes the joint effect sizes for the m genes. We ignore the intercept term considering Y to be mean-centered. We note that $\hat{\mathbf{G}}$ is an estimate of true \mathbf{G} and involves some uncertainty (due to variability in \hat{W}) which is ignored in a standard TWAS. Here, \mathbf{e} denotes the error term and we assume that $E(\mathbf{e}) = \mathbf{0}$, $\text{cov}(\mathbf{e}) = \sigma_e^2 I_{n \times n}$. The joint ordinary least square (OLS) estimate of $\boldsymbol{\alpha}$ is given by: $\hat{\boldsymbol{\alpha}} = (\hat{\mathbf{G}}'\hat{\mathbf{G}})^{-1}\hat{\mathbf{G}}'Y$. We note that an OLS estimate of $\boldsymbol{\alpha}$ should be reliable, because the number of locally heritable genes on a single chromosome (e.g., 500) is expected to be much smaller than the sample size of a contemporary GWAS data (e.g., 10,000). In the standard TWAS, we consider a univariate regression: $E(Y) = \hat{G}_j\gamma_j$, where \hat{G}_j denotes the predicted genetic component of j^{th} gene's expression (j^{th} column of $\hat{\mathbf{G}}$). We test for a marginal association, $H_0 : \gamma_j = 0$ vs $H_1 : \gamma_j \neq 0$. OLS estimate of γ_j is given by: $\hat{\gamma}_j = (\hat{G}_j'\hat{G}_j)^{-1}\hat{G}_j'Y = \frac{\hat{G}_j'Y}{\hat{G}_j'\hat{G}_j}$ with s.e. $(\hat{\gamma}_j) = \frac{\hat{\sigma}_y^2}{\sqrt{\hat{G}_j'\hat{G}_j}}$. Assuming that Y is normalized to have a mean zero and variance one, the Z statistic for testing the marginal association is given by: $z_j = \frac{\hat{G}_j'Y}{\sqrt{\hat{G}_j'\hat{G}_j}}$. We aim to develop our method based on marginal TWAS statistics which are often publicly available.

Expectation of the vector of marginal TWAS statistics

We derive the expectation of marginal TWAS statistics considering the joint model of Y in equation 2: $E(Y) = \hat{\mathbf{G}}\boldsymbol{\alpha}$. Thus,

$$E(z_j) = \frac{\hat{G}_j'E(Y)}{\sqrt{\hat{G}_j'\hat{G}_j}} = \frac{\hat{G}_j'\hat{\mathbf{G}}\boldsymbol{\alpha}}{\sqrt{\hat{G}_j'\hat{G}_j}} \quad (3)$$

Define the diagonal matrix $M_1 = \text{diag}(\frac{1}{\sqrt{\hat{G}_1'\hat{G}_1}}, \dots, \frac{1}{\sqrt{\hat{G}_m'\hat{G}_m}})$. $\hat{\mathbf{G}}'\hat{\mathbf{G}} = \hat{W}'X'X\hat{W} = n\hat{W}'V\hat{W}$. $V = \frac{1}{n}X'X$ is the LD matrix for the r SNPs in GWAS data. Considering the vector of marginal Z statistics across m genes simultaneously, we obtain that:

$$E(Z) = M_1\hat{\mathbf{G}}'\hat{\mathbf{G}}\boldsymbol{\alpha} = nM_1\hat{W}'V\hat{W}\boldsymbol{\alpha} \quad (4)$$

Since $\hat{\mathbf{G}}'\hat{\mathbf{G}} = n\hat{W}'V\hat{W}$, j^{th} diagonal element of $\hat{\mathbf{G}}'\hat{\mathbf{G}}$ is given by: $\hat{G}_j'\hat{G}_j = n[\hat{W}'V\hat{W}]_{jj}$. We define a diagonal matrix, the diagonal entries of which are the diagonal elements of $\hat{W}'V\hat{W}$: $\text{diag}(\hat{W}'V\hat{W})$

$= \text{diag}([\hat{W}'V\hat{W}]_{11}, \dots, [\hat{W}'V\hat{W}]_{mm})$. Thus, $M_1 = \frac{1}{\sqrt{n}} \sqrt{\{\text{diag}(\hat{W}'V\hat{W})\}^{-1}}$. Hence,

$$E(Z) = \sqrt{\{\text{diag}(\hat{W}'V\hat{W})\}^{-1}} \hat{W}'V\hat{W}(\sqrt{n}\boldsymbol{\alpha}) \quad (5)$$

We denote $\boldsymbol{\lambda} = \sqrt{n}\boldsymbol{\alpha}$, $M_2 = \sqrt{\{\text{diag}(\hat{W}'V\hat{W})\}^{-1}}$, and $S = \hat{W}'V\hat{W}$. Thus,

$$E(Z) = M_2S\boldsymbol{\lambda} \quad (6)$$

We note that $\alpha_j = 0$ is equivalent to $\lambda_j = 0$, $j = 1, \dots, m$.

Covariance matrix of the vector of marginal TWAS statistics

We have $Z = \frac{1}{\sqrt{n}}M_2\hat{G}'Y = \frac{1}{\sqrt{n}}M_2\hat{G}'(\hat{G}\boldsymbol{\alpha} + \hat{G}\boldsymbol{\epsilon})$. It can be derived that:

$$\text{cov}(Z) = M_2SM_2, \text{ where } M_2 = \sqrt{\{\text{diag}(\hat{W}'V\hat{W})\}^{-1}} \text{ and } S = \hat{W}'V\hat{W} \quad (7)$$

We note that for a vector of Z statistics, the correlation matrix is the same as the covariance matrix. The full covariance matrix for all chromosomes will be a block-diagonal matrix, where each block corresponds to each chromosome. The inverse of a block-diagonal matrix will again be a block-diagonal matrix containing the corresponding inverted sub-matrices. We also note that two genes on a single chromosome residing far apart (e.g., > 2 MB) are likely to have a zero correlation. This induces a sliding-window type of covariance structure for the genes on each chromosome.

Continuous spike and slab prior

Our main goal is simultaneously estimating the gene-level polygenicity and the optimal subset of non-null genes under a unified Bayesian framework. We consider a Bayesian approach based on continuous spike and slab prior ([9, 12]), where the spike component represents a null effect, and the slab component represents a non-null effect. As mentioned above, we first describe the method for a set of m genes on a single chromosome which can easily be extended to all chromosomes. From previous sections we have: $E(Z) = M_2S\boldsymbol{\lambda}$ and $\text{cov}(Z) = M_2SM_2$, where $M_2 = \sqrt{\{\text{diag}(\hat{W}'V\hat{W})\}^{-1}}$ and $S = \hat{W}'V\hat{W}$. Note that the Z statistic for each gene follows normal. We assume that the vector of Z statistics follows a multivariate normal distribution.

$$Z|\boldsymbol{\lambda} \sim N_m(M_2S\boldsymbol{\lambda}, M_2SM_2) \quad (8)$$

We consider a continuous spike and slab prior distribution for $\boldsymbol{\lambda}$, the vector of TWAS effect sizes for m genes. For $j = 1, \dots, m$, we consider the prior of λ_j as:

$$\begin{aligned} \lambda_j | c_j, \nu &\sim (1 - c_j)N(0, \sigma_0^2) + c_j N(0, \nu^2 \sigma_0^2); \nu \gg 1, \sigma_0^2 = 10^{-10} \\ P(c_j = 1|p) &= p, P(c_j = 0|p) = 1 - p \\ p | a_1, a_2 &\sim \text{Beta}(a_1, a_2) \\ \nu^2 \sigma_0^2 = \sigma_1^2 &\sim \text{Inverse Gamma}(b_1, b_2) \end{aligned} \tag{9}$$

The latent variable c_j defines whether the j^{th} gene has a non-zero effect or not. When $c_j = 0$, $\lambda_j \sim N(0, \sigma_0^2)$, and when $c_j = 1$, $\lambda_j \sim N(0, \nu^2 \sigma_0^2)$. We consider a very small fixed value of $\sigma_0^2 = 10^{-10}$ and a relatively much larger value of $\sigma_1^2 = \nu^2 \sigma_0^2$ (e.g., 10) such that $\nu = \frac{\sigma_1}{\sigma_0} \gg 1$. Since σ_0^2 is nearly zero, if $c_j = 0$, λ_j would be very small which can safely be considered as zero (j^{th} gene is null). We can consider a sufficiently large value of σ_1^2 such that, if $c_j = 1$, λ_j can be treated as non-zero (j^{th} gene is non-null). We refer to σ_0^2 as the spike variance and σ_1^2 as the slab variance. A random variable following $N(0, 10^{-10})$ has 99% probability of taking a value between $(-2.6 \times 10^{-5}, 2.6 \times 10^{-5})$. The proportion of non-null genes, p , measures the gene-level polygenicity. The vector of latent variables, $C = (c_1, \dots, c_m)$, defines the subset of non-null genes which have a non-zero effect on the trait.

For convenience we assume that $\lambda_1, \dots, \lambda_m$ are independently distributed in the prior. Conditioned on p , the configuration indicators (c_1, \dots, c_m) are i.i.d. Bernoulli(p), where $p \sim \text{Beta}(a_1, a_2)$. We assume that $\sigma_1^2 \sim \text{Inverse Gamma}(b_1, b_2)$. We discuss a method of moments approach to choose the hyperparameters (a_1, a_2) and (b_1, b_2) in a later section. We perform a fully Bayesian inference on the gene-level polygenicity and the optimal subset of non-null genes. Note that when $\sigma_0^2 = 0$, the prior has a positive mass at $\lambda_j = 0$, and is known as Dirac spike and slab prior ([12]).

MCMC

We implement the Markov Chain Monte Carlo (MCMC) algorithm using Gibbs sampling to generate a posterior sample of the model parameters. We provide the full-conditional posterior distributions in the following. In a given MCMC iteration, we update $\boldsymbol{\lambda}, C, p, \sigma_1^2$ sequentially.

Full-conditional posterior distribution of $\boldsymbol{\lambda}$: Define D_C to be a diagonal matrix with its j^{th} diagonal element defined in the following way: if $c_j = 0$, it is chosen as σ_0^2 and if $c_j = 1$, it is chosen as σ_1^2 . Thus, the diagonal entries of D_C are $(\sigma_{c_1}^2, \dots, \sigma_{c_m}^2)$. We obtain the full-conditional posterior distribution of $\boldsymbol{\lambda}$ as:

$$\boldsymbol{\lambda} | Z, C, p, \sigma_1^2 \sim N_m(\boldsymbol{\mu}, \Sigma), \text{ where } \Sigma = (S + D_C^{-1})^{-1} \text{ and } \boldsymbol{\mu} = \Sigma M_2^{-1} Z$$

Full-conditional posterior distribution of C : Let $C_{-j} = (c_1, \dots, c_{j-1}, c_{j+1}, \dots, c_m)$. We update the

configuration indicators using the full-conditional distribution of $c_j, j = 1, \dots, m$.

$$P(c_j = 0 | C_{-j}, Z, \boldsymbol{\lambda}, p, \sigma_1^2) = \frac{1}{1 + \frac{p}{1-p} \frac{f(\lambda_j | c_j=1)}{f(\lambda_j | c_j=0)}}$$

Here, $f(\lambda_j | c_j = 1) = N(\lambda_j; 0, \sigma_1^2)$ and $f(\lambda_j | c_j = 0) = N(\lambda_j; 0, \sigma_0^2)$. $N(x; \mu, \sigma^2)$ denotes the normal density at x given μ, σ^2 to be the mean and variance. $P(c_j = 1 | C_{-j}, Z, \boldsymbol{\lambda}, p, \sigma_1^2) = 1 - P(c_j = 0 | C_{-j}, Z, \boldsymbol{\lambda}, p, \sigma_1^2)$.

Full-conditional posterior distribution of p : Denote $m_1 = \#\{c_j | c_j = 1, j = 1, \dots, m\} = \sum_{j=1}^m c_j$ and $m_0 = m - m_1$. We update p from: $p | Z, \boldsymbol{\lambda}, C, \sigma_1^2 \sim \text{Beta}(a_1 + m_1, a_2 + m_0)$.

Full-conditional posterior distribution of σ_1^2 : Next, we update the slab variance σ_1^2 using the following Inverse-Gamma distribution: $\sigma_1^2 | Z, \boldsymbol{\lambda}, C, p \sim \text{Inverse-Gamma}(b_1 + \frac{m_1}{2}, b_2 + \frac{1}{2} \sum_{j:c_j=1} \lambda_j^2)$. Note that, if $m_1 = 0$, σ_1^2 is updated from its prior, Inverse-Gamma(b_1, b_2).

Posterior inference

After a certain burn-in period of the MCMC, we collect the posterior sample of model parameters. We obtain various posterior summaries based on the MCMC sample. We use the posterior median of p as the point estimate of the gene-level polygenicity. We consider a 5% – 95% central posterior interval of p to evaluate the uncertainty in the estimate. In a given MCMC iteration, the vector of latent variables $C = (c_1, \dots, c_m)$ defines the subset of non-null genes. For $j = 1, \dots, m$, $c_j = 1$ implies that the j^{th} gene is included in the subset, and $c_j = 0$ implies that it is excluded. We consider the subset of non-null genes, observed with the maximum frequency in the posterior sample, as an estimate of the optimal subset of non-null genes (maximum a posteriori (MAP) estimate).

Choice of the hyperparameters

We adopt a method of moments (MOM) approach to choosing the hyperparameters in the prior distributions of p and σ_1^2 . To estimate gene-level polygenicity, we focus on the TWAS data obtained from the tissue type that is most relevant for the trait. However, if expression data are available for other tissues in the reference panel (e.g., GTEx data), we can obtain TWAS statistics for different tissue types. We consider the trait’s TWAS data from a closely relevant tissue to estimate the hyperparameters. For example, if we consider the brain the primary tissue type of interest for BMI, we can use the adipose-specific TWAS statistics to estimate the hyperparameters. This is a partially empirical Bayes approach because we use the same GWAS data while computing the TWAS statistics for both the tissue types.

The two shape parameters in the Beta prior of p are a_1, a_2 , and the shape and scale parameters in the inverse-gamma prior of σ_1^2 are b_1, b_2 . For j^{th} gene, we integrate out λ_j to obtain the distribution

of the TWAS statistics conditioned only on p, σ_1^2 : $z_j|p, \sigma_1^2 \sim pN(0, 1 + \sigma_1^2) + (1 - p)N(0, 1)$. Note that the variance of z_j corresponding to the spike component is $(1 + 10^{-10})$ which we approximate as 1. We can derive the k^{th} order raw population moment as $E(z_j^k) = E_p E(z_j^k|p)$, where $E(z_j^k|p) = E_{\sigma_1^2} E(z_j^k|p, \sigma_1^2)$. Here, $E_{\sigma_1^2} E(z_j^k|p, \sigma_1^2) = pE(z_j^k|z_j \sim N(0, 1 + \sigma_1^2)) + (1 - p)E(z_j^k|z_j \sim N(0, 1))$. The odd order moments of z_j are zero, because the distribution of z_j is symmetric at zero conditioned on p, σ_1^2 . Thus, $E(z_j) = E(z_j^3) = 0$. We obtain the second and fourth order moments of z_j as the following:

$$E(z_j^2) = 1 + \frac{a_1}{a_1 + a_2} \frac{b_2}{b_1 - 1}$$

$$E(z_j^4) = 3\left[\frac{a_2}{a_1 + a_2} + \frac{a_1}{a_1 + a_2} \left(1 + \frac{2b_2}{b_1 - 1} + \frac{b_2^2}{(b_1 - 1)(b_1 - 2)}\right)\right]$$

Using the MOM approach we equate $E(z_j^2) = m'_2$ and $E(z_j^4) = m'_4$, where m'_2 and m'_4 are the second and fourth order sample raw moments: $m'_2 = \frac{1}{M} \sum_{j=1}^M z_j^2$ and $m'_4 = \frac{1}{M} \sum_{j=1}^M z_j^4$, where M is the total number of genes on all chromosomes. Since we have two equations in four unknowns, we fix the values of a_1 and b_1 as: $a_1 = 0.1, b_1 = 3$. Then we solve the equations to obtain the choices of a_2 and b_2 . Note that it is challenging and tedious to obtain the sixth and eighth order moments and finally solve for all the four unknowns.

Results

Simulation study

We perform an extensive simulation study to evaluate the efficiency of *polygene* concerning estimating the gene-level polygenicity and the optimal subset of non-null genes. We use the actual genotype data of 337K white-British individuals in the UK Biobank (UKBB) for our simulations.

Simulation design

The software package Fusion [6] analyzed the expression-genotype data in the Young Finish Sequencing (YFS) study to identify all the locally heritable genes in the whole blood tissue. Out of 4700 locally heritable genes, we considered a subset of 2988 genes located in chromosomes 7-22 for our simulations. For each gene, we consider the same set of local SNPs that Fusion included to estimate the local heritability and the prediction model of genetic component of expression. We consider a subset of n_E (e.g., 1000) individuals randomly drawn from the UKBB individuals as the reference panel of expression data. For each gene, we use a linear model to simulate the expression in the reference panel: $E_j = \mathbf{x}'_j \mathbf{w}_j + \epsilon_j$. Here E_j denotes the expression of the j^{th} gene, \mathbf{x}_j denotes the genotypes of the set of local SNPs, and \mathbf{w}_j denotes the corresponding effect sizes. Under the assumption that $V(E_j) = 1$, we consider $\epsilon_j \sim N(0, 1 - h_{e_j}^2)$, where $h_{e_j}^2$ is the local heritability of the expression of j^{th} gene (due to the local SNPs). We assume that a proportion of the local

SNPs affect the expression. If r_{cj} denotes the number of such SNPs, each element of \mathbf{w}_j follows $N(0, \frac{h_{ej}^2}{r_{cj}})$. While simulating the expression, we standardize the genotype data of each local SNP to have zero mean and unity variance. We apply Fusion [6] to simulated data to identify the genes with significant local heritability using a p-value threshold $\frac{0.05}{20000}$. To obtain the prediction model of genetic component of expression, we implement the penalized regression using the elastic net penalty [14] for the expression and local SNPs' genotypes. We only consider the locally heritable genes.

We next simulate the GWAS trait. We randomly select n_{gw} (e.g., 50,000) individuals from UKBB to create the GWAS cohort. We consider the reference panel and GWAS cohort individuals to be non-overlapping. If p is the proportion of non-null genes among m genes, we consider a subset of $m_c = \lceil mp \rceil$ genes to have a non-zero effect on the trait. Suppose expression data is not available in the GWAS. Assuming that the effect size of local SNPs on expression remains the same between the reference panel and the GWAS populations, we denote the true genetic component of expression of j^{th} non-null gene in GWAS as $G_j = X_j' \mathbf{w}_j$, where X_j denotes the genotype vector of the local SNPs in GWAS data, and \mathbf{w}_j denotes the true effect of local SNPs on the expression of j^{th} non-null gene, $j = 1, \dots, m_c$. We simulate $Y = \sum_{j=1}^{m_c} G_j \alpha_j + e$. Assume that $V(Y) = 1$ and the total heritability of Y due to the genetic components of expressions of m_c non-null genes is h_y^2 . Then the random noise $e \sim N(0, 1 - h_y^2)$. We simulate the effect sizes of the non-null genes independently: $\alpha_j \sim N(0, \frac{h_y^2}{m_c})$, $j = 1, \dots, m_c$. We choose the number of non-null genes per chromosome proportional to the number of locally heritable genes in the chromosome. On each chromosome, we consider the approximate LD blocks identified by Berisa and Pickrell [17] such that each block contains at least one heritable gene. We consider a subset of LD blocks randomly selected from a given chromosome and randomly choose a gene from each block to be a non-null gene. In the standard TWAS, we ignore the uncertainty of the predicted genetic component of expression. To evaluate this limitation's impact on *polygene*'s performance, we also performed a TWAS using the actual genetic component of expression in the second stage regression based on the GWAS data. We plug in the true effect sizes of the local SNPs on expression while computing the predicted genetic component of expression in the GWAS data. We refer to this approach as the benchmark TWAS. We compare the performance of *polygene* applied to the standard and benchmark TWAS statistics. For a given dataset, we estimate the hyperparameters to be used in *polygene* based on another dataset generated under the same simulation scenario using the MOM approach discussed above. We used 1000 genome data to estimate the LD structure of SNPs.

In the reference panel, we choose the local heritability of a gene at random between 10% – 15%. We consider 10% of the local SNPs to have a non-zero effect on the expression. We also consider a maximum of 300 SNPs for each gene. While simulating the GWAS trait, we consider a p proportion of locally heritable genes to have a non-null effect on the trait. We chose five different values of $p = 1\%, 2\%, 3\%, 4\%, 5\%$. Thus, for 2988 genes considered on chromosomes 7-22, the maximum

number of non-null genes is considered to be 150. We consider two different choices of the sample size of the reference panel $n_E = 1000, 4000$, and the sample size of the GWAS data as $n_{GW} = 50000$ ($50K$), $70K$ (four different combinations of n_E and n_{GW}). We consider two different scenarios of trait heritability due to predicted expressions. In the first scenario, the heritability increases with the proportion of non-null genes, $10 \times x\%$ heritability due to $x\%$ non-null genes, $x = 1, 2, 3, 4, 5$. In the second scenario, we fix the heritability at 10% and 20%. We run the benchmark TWAS for $n_E = 1000$ and $n_{GW} = 50K$.

Simulation results

Recall that n_E and n_{GW} denote the sample size of the reference panel expression and GWAS data, respectively; p denotes the true proportion of non-null genes; h^2 denotes the trait heritability due to genetic component of expressions. We measure the bias in estimation of p using the relative bias $= \frac{\text{estimated } p - \text{true } p}{\text{true } p}$. In simulation scenarios when h^2 varies in the range of 10% – 20% with $n_{GW} = 50K$ and $n_E = 1000, 4000$, *polygene* provides an accurate estimates of p when its true values are 1%, 2% (Fig 1, Table 1). However, when n_{GW} increases to $70K$ in these scenarios, the upward bias increases (Fig 1, Table 1). In such cases, an increase of n_E helps reduce the upward bias. For example, when $p = 2\%$ and $h^2 = 20\%$ with $n_{GW} = 70K$, an increase of n_E from 1000 to 4000 reduces the mean relative bias from 30% to 24% (Table 1). For validation of *polygene*, we also considered larger values of h^2 with p increasing proportionally. *polygene* produced substantial upward bias in estimated p when h^2 is 30%, 40% and 50% for $p = 3\%, 4\%$ and 5% , respectively (Fig 1). An increase of n_E helped to decrease the upward bias (Fig 1a, Table 1). A possible explanation is that the noise in the predicted expression decreases with an increase of n_E . We also note that in realistic scenarios the heritability of a trait due to genetic component of expressions is limited and not expected to be greater than 20% [18].

Next, we discuss the results when p increases for a fixed h^2 . For $h^2 = 20\%$ and $p = 1\%$, *polygene* produces an upward bias (Table 1), which may be explained by a larger value of mean h^2 per non-null gene. As p increases to 3%, 4%, 5%, the mean heritability per non-null gene becomes smaller, and *polygene* underestimates p (Fig 1, Table 1). Encouragingly, the downward bias diminishes rapidly with an increase of n_{GW} (Fig 2). For example, when $h^2 = 20\%$ and $p = 4\%$ with $n_E = 1000$, the mean relative bias is -9% for $n_{GW} = 70K$ compared to -22% for $n_{GW} = 50K$ (Table 1). In overall, the relative downward bias reduced by 12% – 19% with a mean of 15% due to 20K increase of n_{GW} ($n_E = 1000$). However, the downward bias did not reduce with an increase of n_E (Fig 1b, 1c). The q-value approach [19] which only takes p-values as the input and ignores any possible covariance structure of TWAS statistics produced a very large upward bias while estimating p for most of the simulation scenarios (Table S1).

In standard TWAS, we ignore the uncertainty of predicted expression. To explore the effect of this limitation, we also ran *polygene* for benchmark TWAS in which we plugged in the true effects

of local SNPs on the expression in the second stage regression. We observe that *polygene* based on the benchmark TWAS consistently underestimates p , both in the scenarios of h^2 increasing with p and remaining fixed regardless of p (Fig 3a, 3b, 3c, Table 1). This indicates that the TWAS framework is underpowered in general. Overall, *polygene* estimates p reasonably well, and we can improve the estimation accuracy by increasing the sample sizes of the reference panel expression and GWAS data.

Next, we discuss the usefulness of *polygene* while identifying the optimal subset of non-null genes. We measure the selection accuracy by specificity and sensitivity, where specificity measures the proportion of null genes excluded from the inferred subset, and sensitivity measures the proportion of non-null genes included in the subset. *polygene* produces a very high level of specificity (mean specificity $\geq 95\%$) consistently across the various simulation scenarios (Table 2). It produces a decent overall sensitivity across the scenarios (Table 3). The mean sensitivity is higher when the mean h^2 per non-null gene is higher. For $n_E = 1000$ and $n_{GW} = 50K$, when h^2 increases proportionally to 20%, 30% with $p = 2\%, 3\%$, the mean sensitivity is 50%, 55% compared to 33%, 26% when h^2 is fixed at 10% (Table 3). Thus, the sensitivity decreases with the decrease in the mean heritability per non-null gene.

Sensitivity increases as n_E and n_{GW} increase. For $n_E = 1000$, the mean sensitivity increases when n_{GW} increases from 50K to 70K. For example, for $h^2 = 10\%$ and $p = 2\%$, the mean sensitivity increases from 33% to 40% as n_{GW} increases from 50K to 70K (Table 3). Also, for a given choice of n_{GW} , the mean sensitivity increases when n_E increases. For example, for $n_{GW} = 50K$, $h^2 = 20\%$ and $p = 5\%$, mean sensitivity increases from 34% to 39% when n_E increases from 1000 to 4000 (Table 3). A joint increase in n_E and n_{GW} provides the maximum sensitivity. For example, for $h^2 = 10\%$ and $p = 2\%$, *polygene* produces a maximum of 44% mean sensitivity (Table 3) when both the choices of n_E and n_{GW} are largest ($n_E = 4000$ and $n_{GW} = 70K$). *polygene* based on the benchmark TWAS consistently produces a marginally higher (1 – 3%) specificity compared to standard TWAS (Table 2) at the expense of a marginally lower sensitivity (1% – 3%) in some simulation scenarios (Table 3). In overall, *polygene* performs well to identify the subset of non-null genes with good accuracy.

Real data application

We applied *polygene* to seven phenotypes in UK Biobank (UKBB), three anthropometric traits, three lipid traits, and a case-control trait. We analyzed chromosomes 1-22 together while integrating expression prediction models available from the software package Fusion [6] which were fitted for various tissue types in different expression panels. For each trait, we considered a primary and a secondary tissue type. We use the TWAS statistics based on the secondary tissue type to implement the MOM approach to estimate the hyperparameters in the Bayesian framework of *polygene*. We finally implement *polygene* based on the trait’s TWAS data obtained from the primary tissue type.

Finucane et al. [20] developed a novel method to identify the relevant tissue or cell types for a complex trait and reported the most appropriate tissue types for a collection of traits. Their findings guide the choice of the tissue types pertinent to the traits considered in our analysis. For example, while analyzing a lipid trait (LDL, HDL, or triglyceride), we considered the liver tissue primary and whole blood secondary tissue type. Similarly, for WHR, we considered adipose as the primary tissue and muscle-skeletal as the secondary tissue type. We note that Finucane et al. [20] reported both of these tissue types as significantly relevant for WHR ([20]). We considered the GTEx expression data for most traits, except whole blood in Young Finish Study (YFS) for asthma as the primary tissue type.

In our analysis, height appeared to be most polygenic (posterior median of p as 23% with the 95% central posterior interval as (21%, 25%)) (Table 4). For the other two anthropometric traits, BMI is 11% polygenic with a posterior interval of 9% – 12%, and WHR is 7% polygenic with a posterior interval of 6% – 8% (Table 4). Among the lipids, HDL is the most polygenic (10%), and LDL is the least polygenic (2%) with triglycerides falling between (7%). The point estimates and the posterior intervals of p did not overlap between HDL and LDL, as well as triglycerides and LDL (Table 4). This suggests that HDL and triglycerides are more polygenic than LDL. In our analysis, the case-control trait asthma turned out to be the least polygenic (0.2%).

For each trait analyzed, we also report the optimal subset of non-null genes identified by *polygene* (Table S2 - S10). While the subset for height contains 300 genes (Table S8, S9, S10), the subset for asthma contains five genes (Table S2). Many of the genes included in the optimal subset for a trait were previously reported to be associated with the trait or other relevant traits. For each trait, we mention such a gene in the following. For asthma, QSOX1 on chromosome 1 (Table S2) has been reported to be associated with blood protein measurements [21]. For lipid traits, CELSR2 on chromosome 1 (Table S3, S4, S5) is previously known to be associated with lipids (numerous studies reported in EBI GWAS catalog). For BMI, PPP2R3A on chromosome 3 (Table S6) has been reported to be associated with BMI [22] in the EBI GWAS catalog. For WHR, GRK4 on chromosome 4 (Table S7) is previously known to be associated with BMI-adjusted hip circumference [23]. For height, PEX1 on chromosome 7 (Table S9) is known to be associated with height [24] and other anthropometric traits.

Discussion

We propose a Bayesian approach *polygene* to estimate the gene-level polygenicity for a complex trait under the framework of TWAS. *polygene* simultaneously provides an optimal subset of non-null genes for the trait. It explicitly accounts for the covariance structure between the genes. The method uses summary-level TWAS association statistics which are often publicly available. Along with the point estimate of gene-level polygenicity, *polygene* provides a posterior interval to assess the uncertainty.

The simulation study shows that *polygene* performs well in estimating the proportion of non-null genes in realistic scenarios. When it produces an upward bias (for large values of trait heritability), increasing the sample size of the reference panel expression data helps reduce the bias. The downward bias produced by *polygene* when the heritability per non-null gene is small diminishes rapidly with the increase of the GWAS sample size. For computational convenience, we experimented with a maximum GWAS sample size of 70K in simulations. The relative downward bias decreased by an average of 15% due to a GWAS sample size increase of 20K. With the sample size of contemporary GWASs available (e.g., hundreds of thousands in UK Biobank), we anticipate that the downward bias will reduce substantially. In simulations, we considered the choices of p as 1% – 5%. If we increase p for a fixed h^2 , the magnitude of downward bias will increase due to a decrease in the mean trait heritability per non-null gene. For h^2 proportionally increasing with p , *polygene* is expected to perform well. Consistent downward bias in estimated gene-level polygenicity observed using the benchmark TWAS indicates that the TWAS framework may be underpowered. It also suggests that some portion of the upward bias produced by *polygene* while using the standard TWAS may be due to the lack of uncertainty adjustment in the predicted expression.

polygene performs well while identifying the optimal subset of non-null genes. The estimated subsets are highly specific, with an overall good level of sensitivity. The sensitivity improves if the sample size of the reference panel expression and GWAS data increase. Simulations show that the selection accuracy of *polygene* is comparable between standard and benchmark TWAS. Thus, functional studies can further investigate the optimal subset of non-null genes identified for a complex trait.

While developing the Bayesian method, we also experimented with the Dirac spike and slab prior (point mass at zero). Our preliminary simulations showed that the MCMC implementation does not perform robustly, particularly for many genes (in thousands). We also found that the MCMC for the continuous spike and slab prior is computationally faster than that for the Dirac spike and slab prior. We implemented a method of moments (MOM) approach to choose the hyperparameters in the model based on a tissue type closely relevant to the trait. We propose using the TWAS statistics from a tissue type nearly appropriate to the trait. If the data for a secondary tissue type is unavailable, we can always apply the MOM approach for the primary tissue (an entirely empirical Bayes approach). We have described *polygene* for a continuous trait. However, the method can be applied to a binary trait as well, mainly because the form of the covariance matrix for marginal TWAS statistics depends on the expression prediction model obtained from the reference panel and the LD matrix of the eQTLs. Focus [25] is a fine-mapping method under the TWAS framework which also considers covariance between the TWAS statistics. We note that the analytical form of covariance is similar between Focus and *polygene*. In this paper, we use the term ‘non-null gene’ instead of a ‘causal gene’. The genetic component of the expression of a non-null gene has a non-zero effect on the trait. Our definition does not implicate a formally causal

biological relationship between the non-null gene and the trait. In future work, we plan to estimate the gene-level polygenicity while adjusting for the uncertainty of predicted expression in TWAS.

In summary, *polygene* is a methodologically sound unified Bayesian approach to estimating the gene-level polygenicity and optimal subset of non-null genes for a complex trait under the TWAS framework. It is computationally efficient and can be applied to various traits to understand their genetic architecture better.

Data availability

The datasets that we have analyzed in this paper are available (either openly or via applications) from the following websites:

UK Biobank: <https://www.ukbiobank.ac.uk/>

GTEx: <https://gtexportal.org/home/>

Fusion: <http://gusevlab.org/projects/fusion/>

Acknowledgments

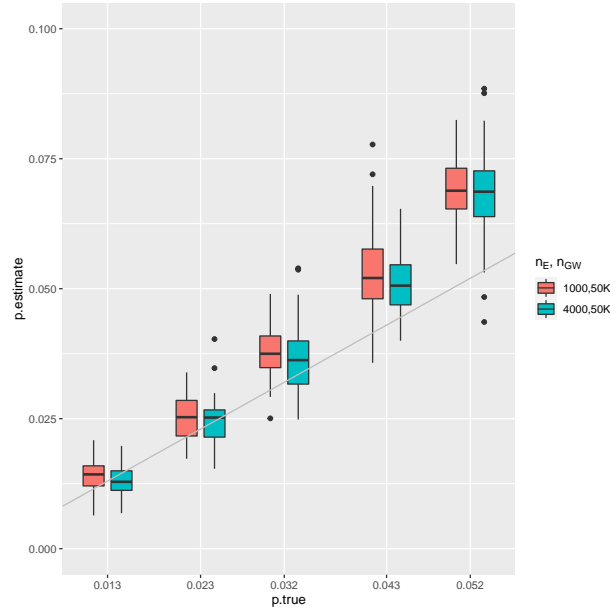
We acknowledge Dr. Nicholas Mancuso for helpful discussions related to this work. We sincerely thank Dr. Tanushree Haldar for helping with the graphical presentation of the paper. This research was conducted using the UK Biobank resource under applications 33297 and 33127.

References

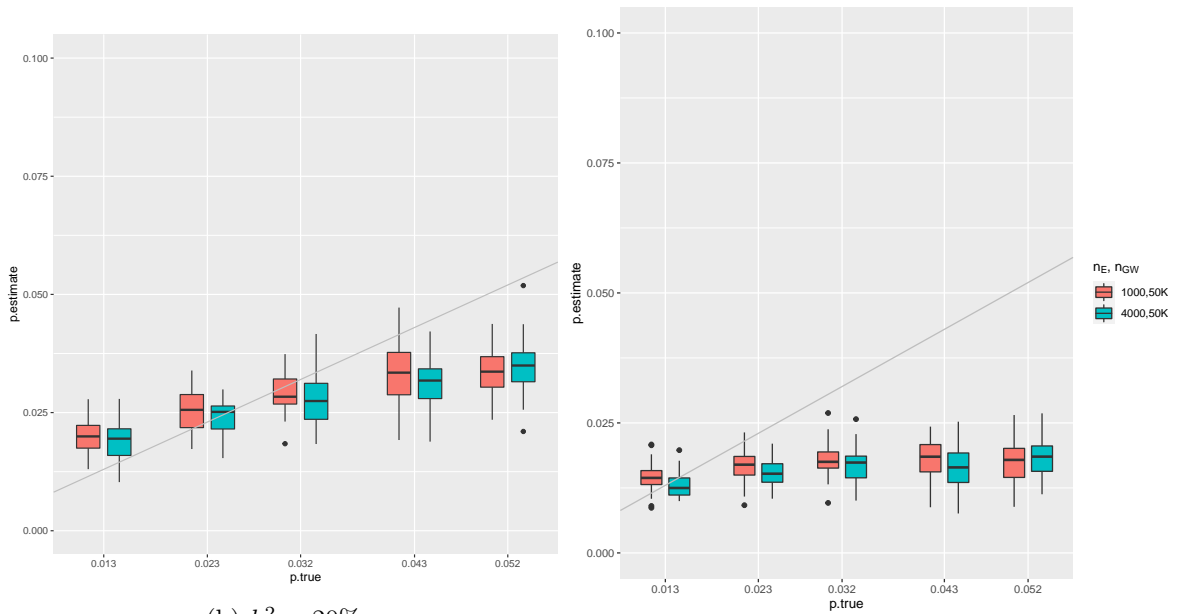
- [1] Yan Zhang, Guanghao Qi, Ju-Hyun Park, and Nilanjan Chatterjee. Estimation of complex effect-size distributions using summary-level statistics from genome-wide association studies across 32 complex traits. *Nature Genetics*, 50(9):1318–1326, 2018.
- [2] Nilanjan Chatterjee, Bill Wheeler, Joshua Sampson, Patricia Hartge, Stephen J Chanock, and Ju-Hyun Park. Projecting the performance of risk prediction based on polygenic analyses of genome-wide association studies. *Nature Genetics*, 45(4):400–405, 2013.
- [3] Luke J O’Connor, Armin P Schoech, Farhad Hormozdiari, Steven Gazal, Nick Patterson, and Alkes L Price. Extreme polygenicity of complex traits is explained by negative selection. *The American Journal of Human Genetics*, 105(3):456–476, 2019.
- [4] Ruth Johnson, Kathryn S Burch, Kangcheng Hou, Mario Paciuc, Bogdan Pasaniuc, and Sriram Sankararaman. Estimation of regional polygenicity from gwas provides insights into the genetic architecture of complex traits. *PLoS computational biology*, 17(10):e1009483, 2021.

- [5] Eric R Gamazon, Heather E Wheeler, Kanaan P Shah, Sahar V Mozaffari, Keston Aquino-Michaels, Robert J Carroll, Anne E Eyler, Joshua C Denny, Dan L Nicolae, Nancy J Cox, et al. A gene-based association method for mapping traits using reference transcriptome data. *Nature genetics*, 47(9):1091, 2015.
- [6] Alexander Gusev, Arthur Ko, Huwenbo Shi, Gaurav Bhatia, Wonil Chung, Brenda WJH Penninx, Rick Jansen, Eco JC De Geus, Dorret I Boomsma, Fred A Wright, et al. Integrative approaches for large-scale transcriptome-wide association studies. *Nature genetics*, 48(3):245, 2016.
- [7] Nicholas Mancuso, Simon Gayther, Alexander Gusev, Wei Zheng, Kathryn L Penney, Zsofia Kote-Jarai, Rosalind Eeles, Matthew Freedman, Christopher Haiman, and Bogdan Pasaniuc. Large-scale transcriptome-wide association study identifies new prostate cancer risk regions. *Nature communications*, 9(1):1–11, 2018.
- [8] Katherine M Siewert-Rocks, Samuel S Kim, Douglas W Yao, Huwenbo Shi, and Alkes L Price. Leveraging gene co-regulation to identify gene sets enriched for disease heritability. *The American Journal of Human Genetics*, 109(3):393–404, 2022.
- [9] Edward I George and Robert E McCulloch. Variable selection via gibbs sampling. *Journal of the American Statistical Association*, 88(423):881–889, 1993.
- [10] Hemant Ishwaran and J Sunil Rao. Spike and slab variable selection: frequentist and bayesian strategies. *The Annals of Statistics*, 33(2):730–773, 2005.
- [11] Veronika Ročková. Bayesian estimation of sparse signals with a continuous spike-and-slab prior. *The Annals of Statistics*, 46(1):401–437, 2018.
- [12] Gertraud Malsiner-Walli and Helga Wagner. Comparing spike and slab priors for bayesian variable selection. *arXiv preprint arXiv:1812.07259*, 2018.
- [13] Robert Tibshirani. Regression shrinkage and selection via the lasso. *Journal of the Royal Statistical Society: Series B (Methodological)*, 58(1):267–288, 1996.
- [14] Hui Zou and Trevor Hastie. Regularization and variable selection via the elastic net. *Journal of the royal statistical society: series B (statistical methodology)*, 67(2):301–320, 2005.
- [15] GTEx Consortium et al. The genotype-tissue expression (gtex) pilot analysis: multitissue gene regulation in humans. *Science*, 348(6235):648–660, 2015.
- [16] GTEx Consortium et al. Genetic effects on gene expression across human tissues. *Nature*, 550(7675):204, 2017.

- [17] Tomaz Berisa and Joseph K Pickrell. Approximately independent linkage disequilibrium blocks in human populations. *Bioinformatics*, 32(2):283, 2016.
- [18] Douglas W Yao, Luke J O’connor, Alkes L Price, and Alexander Gusev. Quantifying genetic effects on disease mediated by assayed gene expression levels. *Nature genetics*, 52(6):626–633, 2020.
- [19] John D Storey. The positive false discovery rate: a bayesian interpretation and the q-value. *The annals of statistics*, 31(6):2013–2035, 2003.
- [20] Hilary K Finucane, Yakir A Reshef, Verneri Anttila, Kamil Slowikowski, Alexander Gusev, Andrea Byrnes, Steven Gazal, Po-Ru Loh, Caleb Lareau, Noam Shores, et al. Heritability enrichment of specifically expressed genes identifies disease-relevant tissues and cell types. *Nature genetics*, 50(4):621, 2018.
- [21] Benjamin B Sun, Joseph C Maranville, James E Peters, David Stacey, James R Staley, James Blackshaw, Stephen Burgess, Tao Jiang, Ellie Paige, Praveen Surendran, et al. Genomic atlas of the human plasma proteome. *Nature*, 558(7708):73–79, 2018.
- [22] Zhaozhong Zhu, Yanjun Guo, Huwenbo Shi, Cong-Lin Liu, Ronald Allan Panganiban, Wonil Chung, Luke J O’Connor, Blanca E Himes, Steven Gazal, Kohei Hasegawa, et al. Shared genetic and experimental links between obesity-related traits and asthma subtypes in uk biobank. *Journal of Allergy and Clinical Immunology*, 145(2):537–549, 2020.
- [23] Anne E Justice, Kristin Young, Stephanie M Gogarten, Tamar Sofer, Misa Graff, Shelly Ann M Love, Yujie Wang, Yann C Klimentidis, Miguel Cruz, Xiuqing Guo, et al. Genome-wide association study of body fat distribution traits in hispanics/latinos from the hchs/sol. *Human molecular genetics*, 30(22):2190–2204, 2021.
- [24] Ioanna Tachmazidou, Dániel Süveges, Josine L Min, Graham RS Ritchie, Julia Steinberg, Klaudia Walter, Valentina Iotchkova, Jeremy Schwartzentruber, Jie Huang, Yasin Memari, et al. Whole-genome sequencing coupled to imputation discovers genetic signals for anthropometric traits. *The American Journal of Human Genetics*, 100(6):865–884, 2017.
- [25] Nicholas Mancuso, Malika K Freund, Ruth Johnson, Huwenbo Shi, Gleb Kichaev, Alexander Gusev, and Bogdan Pasaniuc. Probabilistic fine-mapping of transcriptome-wide association studies. *Nature genetics*, 51(4):675–682, 2019.



(a) $h^2 = 10\%, 20\%, 30\%, 40\%, 50\%$



(b) $h^2 = 20\%$

(c) $h^2 = 10\%$

Figure 1: Box plots for estimated polygenicity when trait heritability due to the genetic component of expressions are (a) 10%, 20%, 30%, 40%, 50% for 1%, 2%, 3%, 4%, 5% non-null genes, respectively, (b) fixed at 20%, (c) fixed at 10%. We consider two different choices of the sample size of the expression panel data (n_E) as 1000 and 4000. Here, the GWAS sample size is 50K.

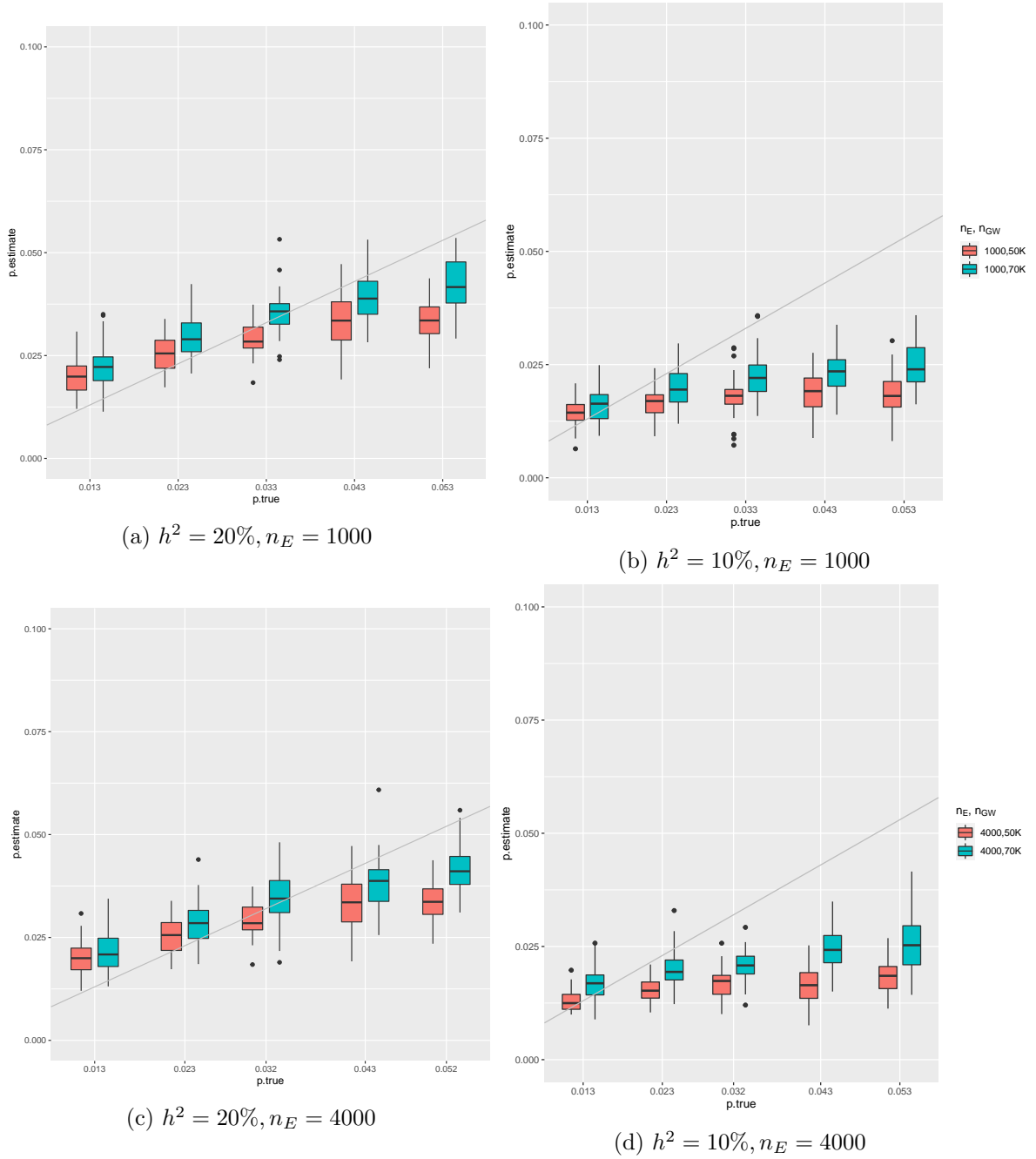
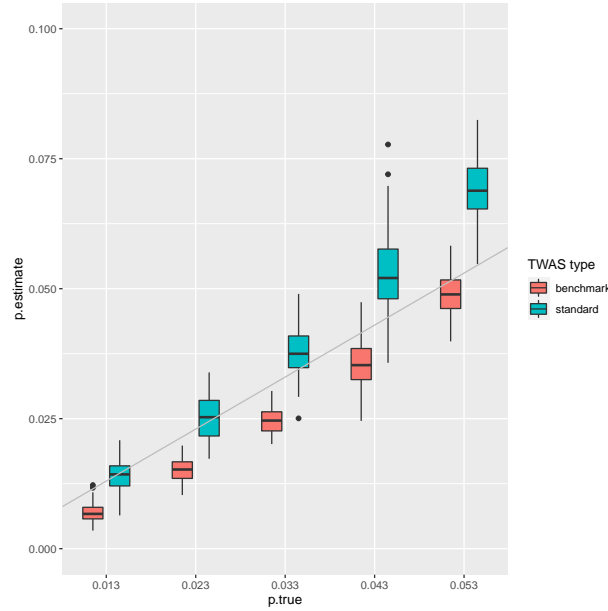
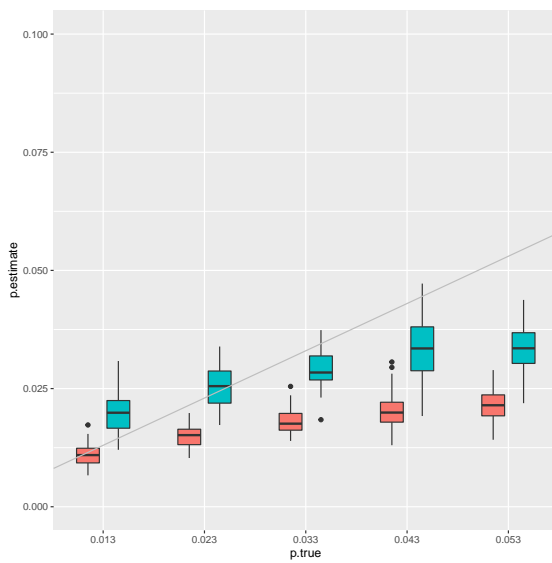


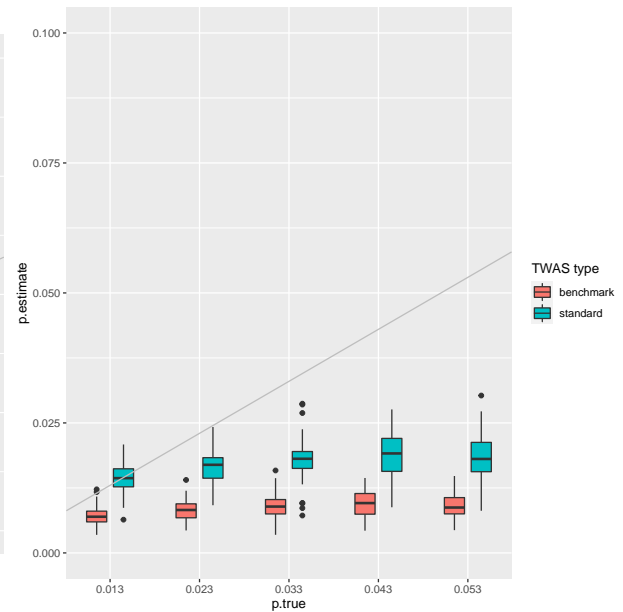
Figure 2: Estimated polygenicity when the GWAS sample size increases from 50K to 70K for a fixed choice of the sample size of reference panel expression data (n_E). In (a) and (b), we fix $n_E = 1000$ and consider the trait heritability due to genetic component of expressions as 20% (a) and 10% (b), respectively. In both scenarios, we increase the GWAS sample size from 50K to 70K. We set $n_E = 4000$ and repeat the same analyses in (c) and (d).



(a) $h^2 = 10\%, 20\%, 30\%, 40\%, 50\%$



(b) $h^2 = 20\%$



(c) $h^2 = 10\%$

Figure 3: Comparison between estimated polygenicity obtained by *polygene* using the benchmark TWAS and standard TWAS when the trait heritability due to genetic component of expressions are (a) 10%, 20%, 30%, 40%, 50% for 1%, 2%, 3%, 4%, 5% non-null genes, respectively, (b) fixed at 20%, (c) fixed at 10%. The sample size of the expression panel and GWAS data are considered as 1000 and 50K, respectively.

Table 1: Percentage of relative bias produced by *polygene* while estimating p using standard TWAS and benchmark TWAS in various simulation scenarios. n_E and n_{GW} denote the sample sizes of the reference panel expression and the GWAS data, respectively.

Simulation		standard TWAS				benchmark TWAS
scenarios		n_E, n_{GW}				n_E, n_{GW}
p	h^2	1000, 50K	1000, 70K	4000, 50K	4000, 70K	1000, 50K
1%	10%	3	25	4	21	-43
2%	20%	6	30	7	24	-33
3%	30%	14	36	13	37	-24
4%	40%	24	41	19	37	-12
5%	50%	31	53	32	49	-6
1%	20%	47	71	48	67	-10
3%	20%	-12	7	-12	7	-43
4%	20%	-22	-9	-26	-12	-51
5%	20%	-37	-20	-33	-20	-59
2%	10%	-32	-13	-31	-16	-61
3%	10%	-47	-32	-47	-32	-70
4%	10%	-57	-45	-57	-44	-75
5%	10%	-65	-53	-63	-52	-80

Table 2: Mean specificity of *polygene* while inferring the subset of non-null genes using standard and benchmark TWAS in various simulation scenarios. n_E and n_{GW} denote the sample sizes of the reference panel expression and the GWAS data, respectively.

Simulation		standard TWAS				benchmark TWAS
scenarios		n_E, n_{GW}				n_E, n_{GW}
p	h^2	1000, 50K	1000, 70K	4000, 50K	4000, 70K	1000, 50K
1%	10%	99	99	99	99	100
2%	20%	99	98	99	99	100
3%	30%	98	97	98	98	99
4%	40%	97	97	97	97	99
5%	50%	96	95	96	96	98
1%	20%	99	99	99	99	100
3%	20%	99	98	99	98	100
4%	20%	98	98	99	98	99
5%	20%	98	98	98	98	100
2%	10%	99	99	99	99	100
3%	10%	99	99	99	99	100
4%	10%	99	99	99	99	100
5%	10%	99	99	99	99	100

Table 3: Mean sensitivity of *polygene* while inferring the subset of non-null genes using standard and benchmark TWAS in various simulation scenarios. n_E and n_{GW} denote the sample sizes of the reference panel expression and GWAS data, respectively.

Simulation scenarios		standard TWAS				benchmark TWAS
		n_E, n_{GW}				n_E, n_{GW}
p	h^2	1000, 50K	1000, 70K	4000, 50K	4000, 70K	1000, 50K
1%	10%	44	51	49	55	43
2%	20%	50	57	53	60	49
3%	30%	55	61	58	64	53
4%	40%	58	64	61	67	58
5%	50%	62	67	65	70	61
1%	20%	61	65	66	69	60
3%	20%	44	52	47	54	42
4%	20%	40	46	42	49	37
5%	20%	34	42	39	45	32
2%	10%	33	40	36	44	30
3%	10%	26	34	30	36	24
4%	10%	22	27	25	32	19
5%	10%	18	24	21	28	16

Table 4: Estimation of gene-level polygenicity by *polygene* for seven phenotypes in UK Biobank integrating external expression panel data. We used the expression prediction models from the Fusion software package. The expression prediction model based on whole blood, considered a primary tissue type for asthma, was collected from the Young Finish Study (YFS). All other expression prediction models used here were fitted in the GTEx study.

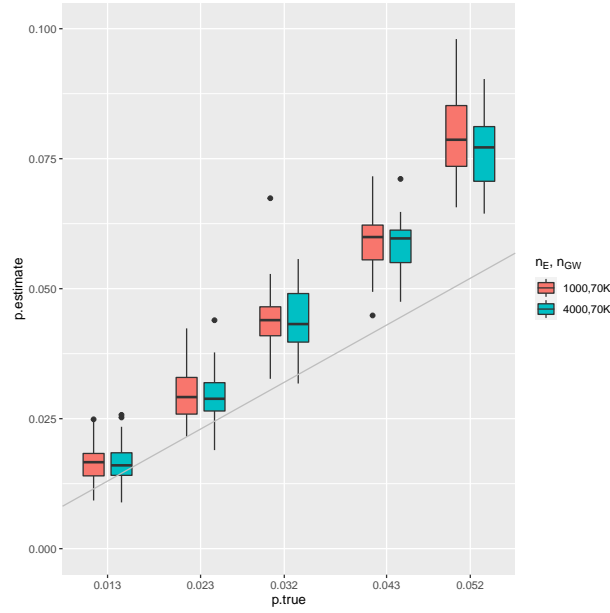
	Estimated polygenicity			Tissue-type	
	Posterior median	95% posterior interval		Primary	Secondary
Height	22.7%	20.9%	24.6%	Muscle skeletal	Adipose subcutaneous
BMI	10.5%	8.8%	12.3%	Brain cerebellum	Adipose subcutaneous
WHR	6.8%	5.8%	7.9%	Adipose subcutaneous	Muscle skeletal
HDL	9.9%	7.4%	12.7%	Liver	Whole blood
Triglycerides	7.0%	5.0%	9.4%	Liver	Whole blood
LDL	1.7%	0.8%	3.1%	Liver	Whole blood
Asthma	0.2%	0.1%	0.4%	Whole blood (YFS)	Whole blood

Supplementary materials: A Bayesian method for estimating
gene-level polygenicity under the framework of transcriptome-wide
association study

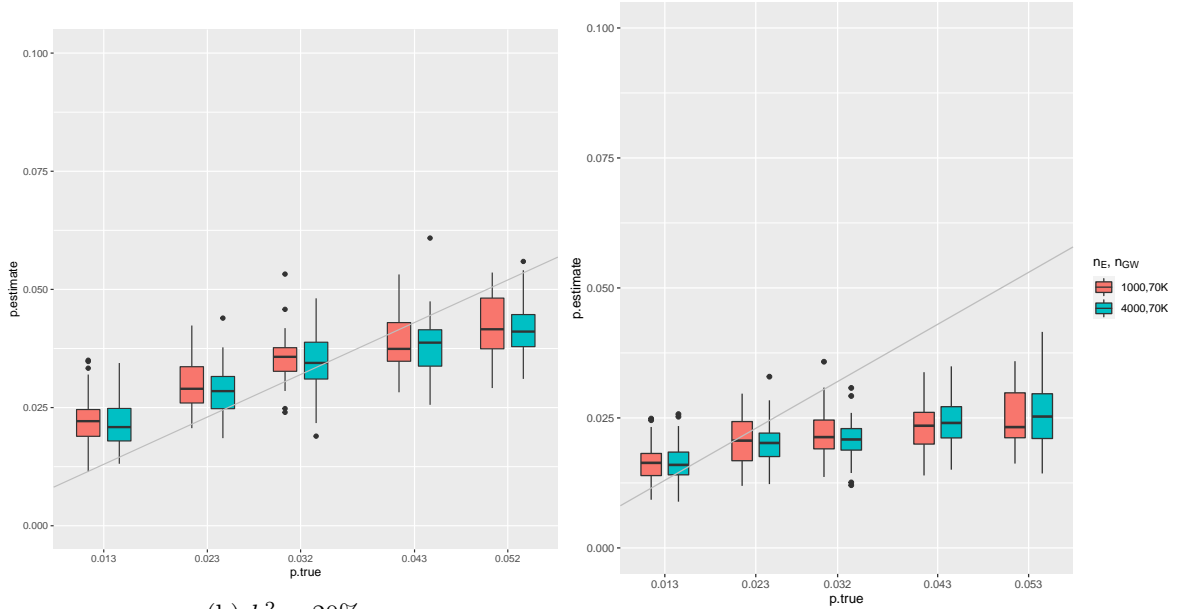
Arunabha Majumdar^{1*} and Bogdan Pasaniuc^{2*}

¹Department of Mathematics, Indian Institute of Technology Hyderabad, Kandi, Telangana, India

²Department of Pathology and Laboratory Medicine, University of California Los Angeles, California, USA



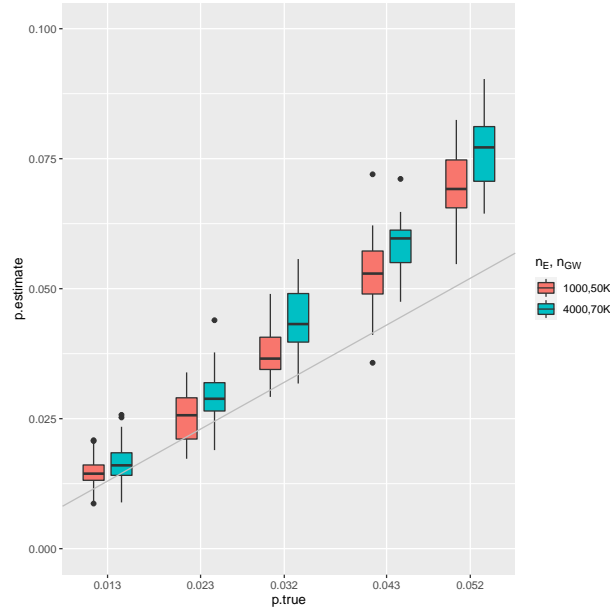
(a) $h^2 = 10\%, 20\%, 30\%, 40\%, 50\%$



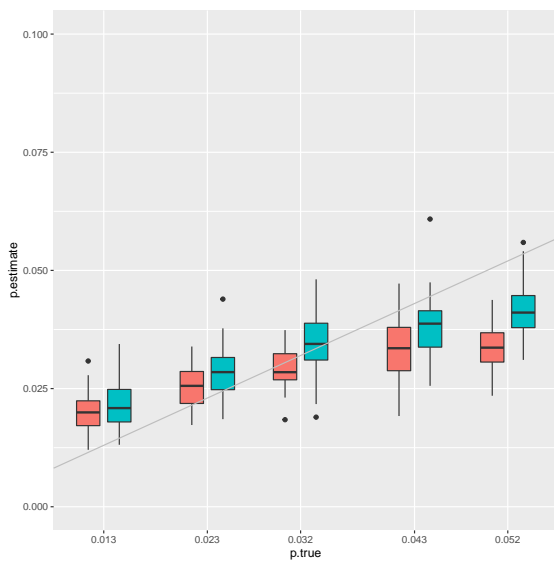
(b) $h^2 = 20\%$

(c) $h^2 = 10\%$

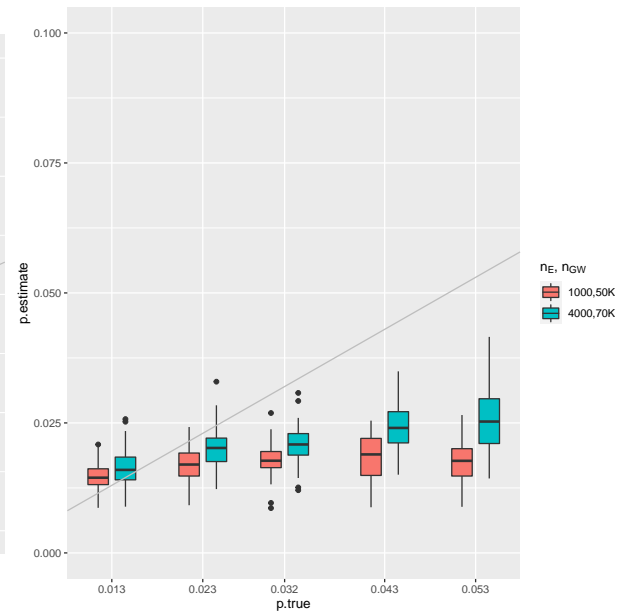
Figure S1: Estimated polygenicity for GWAS sample size $70K$. The trait heritability due to the genetic component of expressions are $10\%, 20\%, 30\%, 40\%, 50\%$ for $1\%, 2\%, 3\%, 4\%, 5\%$ non-null genes, respectively (a), fixed at 20% (b), fixed at 10% (c). We consider two different choices of the sample size of the expression panel data (n_E) as 1000 and 4000 .



(a) $h^2 = 10\%, 20\%, 30\%, 40\%, 50\%$



(b) $h^2 = 20\%$



(c) $h^2 = 10\%$

Figure S2: Estimated polygenicity when the sample size increases for both the reference panel expression and GWAS data. We increase reference panel sample size from 1000 to 4000, and GWAS sample size from 50K to 70K. The trait heritability due to genetic component of expressions are 10%, 20%, 30%, 40%, 50% for 1%, 2%, 3%, 4%, 5% non-null genes, respectively (a), fixed at 20% (b), fixed at 10% (c).

Table S1: Percentage of relative bias produced by the q-value approach while estimating p in various simulation scenarios. The estimated p is based on standard TWAS. n_E and n_{GW} denote the sample sizes of the reference panel expression and GWAS data. We use the following formula of relative bias: $\frac{\text{estimated } p - \text{true } p}{\text{true } p} \times 100$

p	h^2	$n_E = 1000$	$n_E = 1000$	$n_E = 4000$	$n_E = 4000$
		$n_{GW} = 50K$	$n_{GW} = 70K$	$n_{GW} = 50K$	$n_{GW} = 70K$
1%	10%	1149	1202	979	1067
2%	20%	670	699	574	612
3%	30%	459	493	441	445
4%	40%	367	400	355	372
5%	50%	349	340	296	330
1%	20%	1219	1258	971	1131
3%	20%	446	480	403	420
4%	20%	324	348	306	313
5%	20%	267	277	212	251
2%	10%	604	654	567	576
3%	10%	413	438	425	389
4%	10%	302	307	260	260
5%	10%	246	241	179	229

Table S2: Subset of non-null genes for Asthma identified by *polygene*.

CHR	Gene
1	QSOX1
7	PDK4
10	TMEM180
17	CASC3
17	RAPGEFL1

Table S3: Subset of non-null genes for LDL identified by *polygene*.

CHR	Gene
1	CELSR2
2	AC009404.2
3	GNL3
3	RP11-299J3.8
11	SOX6
19	CTB-50L17.9

Table S4: Subset of non-null genes for HDL identified by *polygene*.

CHR	Gene	CHR	Gene
1	CELSR2	10	AGAP4
1	CTSS	11	SOX6
1	CERS2	11	HSD17B12
1	RP11-316M1.12	11	RP11-613D13.5
3	PPM1M	12	GLIPR1L2
3	GNL3	12	RP11-585P4.5
3	RP5-966M1.6	14	GSTZ1
3	RP11-234A1.1	15	RPL9P25
4	RP11-33B1.4	15	WHAMM
5	ARHGEF28	17	NR1D1
5	ERAP2	17	WIPI1
7	AC091729.9	19	ZNF846
7	PILRB	19	SSBP4
7	STAG3L5P-PVRIG2P-PILRB	19	ITPKC
7	PILRA	19	ETHE1
7	RP11-134L10.1	19	ZNF211
8	SNX16	22	BCR

Table S5: Subset of non-null genes for triglycerides identified by *polygene*.

CHR	Gene	CHR	Gene
1	CELSR2	7	RP11-274B21.3
1	CTSS	9	PMPCA
1	CERS2	10	APBB1IP
1	RP11-316M1.12	10	ALDH18A1
3	PPM1M	11	SPTY2D1-AS1
3	GNL3	11	RP11-613D13.5
4	RP11-33B1.4	11	CEP57
4	RP11-33B1.1	14	GSTZ1
7	RP11-274B21.1	15	RPL9P25
7	RP11-274B21.2	15	WHAMM
7	RP11-274B21.4	16	PDXDC2P
7	AC018638.1	19	CTB-50L17.9

Table S6: Subset of non-null genes for BMI identified by *polygene*.

CHR	Gene	CHR	Gene	CHR	Gene	CHR	Gene
1	CROCC	3	PPP2R3A	10	RP11-179B2.2	16	NLRC3
1	MST1L	3	RP11-731C17.2	10	ARL3	16	SLX4
1	RP11-108M9.4	3	RP11-85F14.5	10	LHPP	16	CTD-2033A16.3
1	RP11-108M9.5	3	COMMD2	11	TMEM9B-AS1	16	NOB1
1	PPIE	3	KLHL24	11	ARL14EP	16	PDPR
1	ACADM	3	YEATS2-AS1	11	HSD17B12	16	RP11-296I10.3
1	ECM1	3	ABCC5	11	MRPL11	17	PNPO
1	IRF6	4	GRK4	11	CTD-3074O7.12	17	RP11-6N17.9
1	RP3-434O14.8	4	CISD2	11	MRPL21	17	CDK5RAP3
2	AC092159.2	4	RP11-33B1.4	11	IGHMBP2	17	CALCOCO2
2	FAM228B	4	RP11-33B1.1	11	ARHGAP20	17	NARF
2	TRMT61B	4	ELF2	11	TTC12	19	EVI5L
2	GGCX	5	RNF180	11	HMBS	19	LRRC25
2	MRPS9	7	PMS2P5	12	PPHLN1	19	UPF1
2	PHOSPHO2	7	LAMTOR4	12	RP11-328C8.4	19	ARMC6
2	KLHL23	7	AP1S1	12	PRICKLE1	19	PAF1
2	TTC30A	7	EXOC4	12	RP11-394J1.2	20	GSS
3	EAF1	8	FAM86B3P	12	ZNF605	20	MYH7B
3	CCDC71	8	NTAN1P2	13	MIPEP	20	YWHAB
3	GPX1	8	DPY19L4	14	FAM177A1	21	PSMG1
3	FAM212A	9	C9orf40	14	ZFYVE1	21	BX322557.10
3	GLYCTK	9	C9orf41	15	TIPIN	21	LINC00205
3	ITIH4-AS1	9	NMRK1	15	MAP2K5	22	ZDHHC8
3	IQCB1	9	PRPS1P2	16	CLUAP1		

Table S7: Subset of non-null genes for WHR identified by *polygene*.

CHR	Gene	CHR	Gene	CHR	Gene	CHR	Gene
1	THAP3	3	RP11-85F14.5	10	NOC3L	15	WHAMM
1	MUL1	3	TIPARP-AS1	10	CACUL1	15	UBE2Q2P1
1	ZNHIT6	3	LINC00886	11	RP11-613D13.5	16	MIR940
1	PIGC	4	GRK4	11	RAB30	16	ZNF263
2	UBXN2A	4	TMEM165	11	TMEM126A	16	RP11-266L9.4
2	ADCY3	4	AADAT	11	PGR	17	NAGLU
2	RP11-443B20.1	5	LYSMD3	11	TTC12	17	RP11-400F19.8
2	HOXD-AS1	5	SIL1	11	VPS11	17	CRHR1-IT1
2	NDUFS1	5	PCDHB2	11	HMBS	17	CRHR1
2	AC007383.4	6	RP11-250B2.3	12	POC1B	17	RP11-6N17.6
2	METTTL21A	6	GPR126	12	C12orf52	17	RP11-6N17.10
2	2-Sep	6	RP11-545I5.3	12	ZNF605	17	HOXB2
3	RP11-380O24.1	6	VIP	13	RNASEH2B	17	HOXB-AS1
3	SETD5-AS1	7	INTS1	13	RNF219	17	HOXB3
3	TCTA	7	AC092171.4	14	AL132989.1	17	RP11-147L13.8
3	NICN1	7	SNX10	14	PCNX	18	KATNAL2
3	NICN1-AS1	7	AC004540.4	14	MARK3	19	ANKRD24
3	RNF123	7	BCL7B	14	APOPT1	19	XAB2
3	GNL3	7	MLXIPL	14	RP11-73M18.8	19	ZNF100
3	NEK4	7	AP1S1	14	XRCC3	19	ZNF507
3	TMEM110	7	RP11-514P8.8	14	PPP1R13B	19	PINLYP
3	WDR52	7	POLR2J3	15	GABPB1-AS1	20	TRPC4AP
3	FAM86JP	7	CPED1	15	CTD-3110H11.1	20	EDEM2
3	SLC41A3	7	EXOC4	15	DIS3L	20	PROCR
3	RP11-124N2.1	9	DNLZ	15	TIPIN	20	MMP24
3	PCCB	10	ZCCHC24	15	MAP2K5	20	UQCC1
						22	THOC5

Table S8: Subset of non-null genes for height identified by *polygene*.

CHR	Gene	CHR	Gene	CHR	Gene	CHR	Gene
1	PGD	1	EGLN1	3	NICN1	4	UBE2D3
1	NBPF1	2	SH3YL1	3	NICN1-AS1	4	RP11-33B1.1
1	CROCC	2	ADI1	3	FAM212A	5	C5orf22
1	MST1L	2	AC142528.1	3	NEK4	5	NSA2
1	RP11-108M9.4	2	UBXN2A	3	ITIH4-AS1	5	DHFR
1	RP11-108M9.5	2	PFN4	3	RP5-966M1.6	5	MSH3
1	PADI2	2	HMGB1P31	3	TMEM110	5	GIN1
1	DDOST	2	RP11-493E12.2	3	RFT1	5	PRR16
1	EIF4G3	2	GGCX	3	LNP1	5	ALDH7A1
1	PIGV	2	ZNF514	3	PCCB	5	SRA1
1	FNDC5	2	C2orf49	3	CEP70	5	PCDHB16
1	MEAF6	2	C2orf40	3	ATP1B3	5	PANK3
1	RP11-767N6.7	2	ERCC3	3	PCOLCE2	6	RNF144B
1	IPP	2	AC093388.3	3	PLOD2	6	PRICKLE4
1	MAST2	2	PPIL3	3	RSRC1	6	MED20
1	GBP3	2	NOP58	3	RP11-538P18.2	6	CD2AP
1	CELSR2	2	KCNE4	3	YEATS2-AS1	6	HMG3
1	CHD1L	2	TRAF3IP1	4	Z95704.2	6	RP11-250B2.6
1	RP11-337C18.10	2	NDUFA10	4	HTT	6	DOPEY1
1	ACP6	2	HDLBP	4	QDPR	6	SMIM8
1	POGZ	2	2-Sep	4	DANCR	6	C6orf163
1	FMO4	3	XPC	4	SRD5A3	6	FRK
1	NCF2	3	LSM3	4	SRD5A3-AS1	6	NUS1
1	CDC42BPA	3	CRTAP	4	REST	6	TULP4
1	SNAP47	3	AMT	4	UBA6	6	IGF2R

Table S9: Subset of non-null genes for height identified by *polygene*.

CHR	Gene	CHR	Gene	CHR	Gene	CHR	Gene
7	EIF3B	8	CSGALNACT1	10	PAPSS2	12	C12orf23
7	DPY19L1P1	8	BRF2	10	NOC3L	12	MMAB
7	KBTBD2	8	ADAM9	10	CWF19L1	12	DDX55
7	GUSB	8	RPS20	10	TMEM180	12	EIF2B1
7	GS1-124K5.11	8	DSCC1	10	PRDX3	12	TCTN2
7	GS1-124K5.12	8	WDYHV1	10	PLEKHA1	13	C1QTNF9B-AS1
7	KCTD7	9	RP11-112J3.16	10	JAKMIP3	13	COG6
7	RP11-458F8.2	9	TMEM8B	11	LDHA	14	CTD-2002H8.2
7	TYW1	9	HRCT1	11	TSG101	14	FLVCR2
7	RP11-166O4.5	9	RP11-522I20.3	11	MPPED2	14	RP11-747H7.3
7	POM121B	9	GKAP1	11	AP000442.1	14	TRIP11
7	CYP51A1	9	RMI1	11	MS4A14	14	RP11-529H20.6
7	PEX1	9	CDC20P1	11	CTSF	14	ATXN3
7	ZSCAN21	9	FKBP15	11	TPCN2	14	NDUFB1
7	PILRB	9	CDC26	11	SYTL2	14	ZFYVE21
7	STAG3L5P-PVRIG2P -PILRB	9	GOLGA1	11	MED17	15	C15orf41
7	PILRA	9	PPP6C	11	AP001877.1	15	DIS3L
7	TSC22D4	9	GAPVD1	11	FDX1	15	RP11-352G18.2
7	GIGYF1	9	DNLZ	12	WBP11	15	TIPIN
7	TRIP6	9	CARD9	12	RP11-967K21.1	15	RPL9P25
7	TSPAN33	10	AKR1C2	12	RP11-996F15.2	15	SNAPC5
7	RP11-286H14.6	10	PHYH	12	RP11-611E13.2	15	SMAD3
7	RP4-800G7.2	10	KIF5B	12	MRPL42	15	AP3B2
7	NOM1	10	DNA2	12	CCDC53	15	RP11-182J1.14
8	MFHAS1	10	RPS24	12	CKAP4	15	RN7SL417P

Table S10: Subset of non-null genes for height identified by *polygene*.

CHR	Gene	CHR	Gene	CHR	Gene	CHR	Gene
15	WDR73	17	EFCAB13	19	SUGP1	20	GGT7
15	ALPK3	17	MRPL45P2	19	MAU2	20	ACSS2
15	DET1	17	RP11-6N17.4	19	ZNF714	20	GSS
15	POLG	17	AC003665.1	19	ZNF738	20	MMP24-AS1
15	PEX11A	17	PNPO	19	ZNF493	20	MMP24
16	BRICD5	17	RP11-6N17.6	19	ZNF429	20	RP4-614O4.11
16	ECI1	17	RP5-890E16.2	19	ZNF100	20	EIF6
16	MIR940	17	HOXB3	19	ZNF43	20	UQCC1
16	NTAN1	17	COX11	19	ZNF507	20	YWHAB
16	NPIPA5	17	BZRAP1	19	GPATCH1	20	SNX21
16	ABCC6	17	LRRC37A16P	19	COX6B1	20	PREX1
16	TANGO6	17	CCDC40	19	WDR62	20	B4GALT5
16	PHLPP2	17	GAA	19	TBCB	21	PIGP
16	RFWD3	17	RAB40B	19	LINC00665	21	TTC3
17	ZNF286B	17	FN3KRP	19	ITPKC	21	UBE2G2
17	RP11-173M1.8	18	POLI	19	PHLDB3	21	POFUT2
17	TP53I13	18	CNDP2	19	ETHE1	22	UFD1L
17	RAPGEFL1	19	MPND	19	ZNF575	22	AC000068.10
17	HSD17B1P1	19	AC007292.3	19	SMG9	22	AP000350.4
17	DCAKD	19	CHAF1A	19	DMWD	22	DDT
17	PLCD3	19	CTB-50L17.5	19	FUZ	22	CTA-445C9.15
17	PLEKHM1	19	CTB-50L17.9	19	ZNF667-AS1	22	MTMR3
17	LRRC37A4P	19	KRI1	20	C20orf194	22	PLA2G6
17	CRHR1-IT1	19	SLC44A2	20	CBFA2T2	22	DMC1
17	CRHR1	19	SSBP4	20	MAP1LC3A	22	TOMM22